

Ancilla-Free Quantum Protocol for Thermal Green's Functions

Changhao Yi^{1, 2, 3} and Cunlu Zhou^{4, 5}

¹*State Key Laboratory of Surface Physics, Department of Physics,*

and Center for Field Theory and Particle Physics, Fudan University, Shanghai 200433, China

²*Institute for Nanoelectronic Devices and Quantum Computing, Fudan University, Shanghai 200433, China*

³*Shanghai Research Center for Quantum Sciences, Shanghai 201315, China*

⁴*Department of Computer Science, Université de Sherbrooke, QC, Canada*

⁵*Institut quantique, Université de Sherbrooke, QC, Canada*

(Dated: September 23, 2025)

We introduce a simple and noise-resilient quantum algorithm for computing both zero- and finite-temperature Green's functions, requiring no ancillas and relying only on native time evolution and measurements readily available on current platforms. Exploiting parity symmetry—a condition satisfied by a broad class of Hamiltonians relevant to condensed matter physics and quantum chemistry, including the Fermi–Hubbard and Heisenberg models—we construct symmetric and antisymmetric thermal states and apply a tailored quench spectroscopy scheme to extract the exact real and imaginary parts of two-point time correlators, from which Green's functions are efficiently reconstructed. The protocol is theoretically efficient, experimentally accessible, and directly applicable to both digital and analog quantum computers. Beyond Green's functions, the same framework extends naturally to out-of-time-order correlators (OTOCs). This work highlights a practical path toward probing finite-temperature dynamics of strongly correlated quantum systems on near-term and early fault-tolerant quantum hardware.

Introduction—Green's functions are essential tools for probing strongly interacting many-body systems [1]. They compactly describe the propagation of particles and excitations without explicit wave-function representations, and they encode key information about the density of states and band structure, which underpin phenomena such as superconductivity, magnetism, and phase transitions. Experimentally, techniques like angle-resolved photoemission spectroscopy (ARPES) [2] and resonant inelastic X-ray scattering (RIXS) [3] are well-established for probing Green's functions. On the computational side, classical approaches such as dynamical mean field theory [4], exact diagonalization [5], quantum Monte Carlo [6], and tensor networks [7] have been refined for decades, yet still face exponential worst-case scaling with system size.

Quantum computing offers a promising alternative by enabling direct measurement of time correlators. A wide range of quantum algorithms has been proposed, including using quantum phase estimation [8, 9], local rotation [10], quench spectroscopy [11–14], variational approaches [15, 16], filter function [17, 18], Fourier transform [19, 20], quantum subspace expansion [21, 22], linear response theory [23–25], multiple-observable dynamic mode decomposition [26], and continued fraction representation [27, 28]. Many of these methods use at least one ancilla qubit and some need to perform the Hadamard test [29], but this subroutine introduces significant practical obstacles. In particular, it requires controlled implementations of large unitaries, which greatly increase circuit depth and error rates, while also relying on long-range entangling gates between the ancilla and system qubits. These challenges are

compounded by the fact that controlled operations are among the noisiest available on current platforms, and the ancilla qubit itself must be maintained and measured with high fidelity. As a result, the Hadamard test is especially problematic for experimental implementation in the noisy intermediate-scale quantum (NISQ) era [30] and remains demanding even in the early fault-tolerant regime [31].

In this work, we present an ancilla-free, noise-resilient quantum algorithm based on a *tailored quench spectroscopy* (TQS) protocol for computing both zero- and finite-temperature Green's functions by exploiting *parity symmetry* [1]. Specifically, we consider Hamiltonians that commute with a parity operator P , while the observables of interest A and B anti-commute with P . This condition is satisfied by a broad class of Hamiltonians central to condensed matter physics and quantum chemistry, notably the Fermi–Hubbard and Heisenberg models.

Quench spectroscopy (QS) is a simple yet powerful technique for probing the dynamical properties of quantum systems. By suddenly perturbing an initial state and monitoring its time evolution, one can extract spectral and correlation functions without requiring complex time-dependent controls [12, 13]. A typical QS protocol proceeds as follows: prepare an initial state; apply a sudden change (the quench), often a local operator or global perturbation; let the system evolve under the original Hamiltonian H ; measure an observable over time, where the resulting signal encodes oscillations at frequencies corresponding to energy differences in the system; and finally, analyze the signal to obtain spectral and correlation functions, thereby revealing the system's excitations and dynamical properties. We refer to the expec-

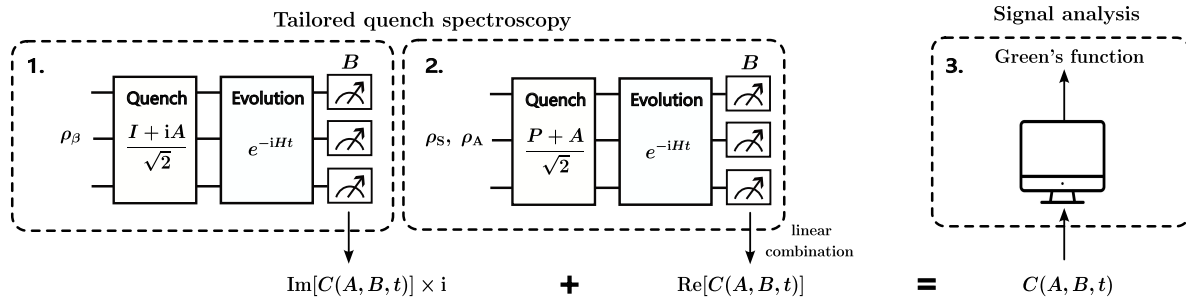


FIG. 1. Procedure for computing finite-temperature Green's functions via tailored quench spectroscopy (TQS). Step 1: Prepare a thermal state ρ_β (e.g., using a quantum Gibbs sampler) and apply TQS to measure two-point time correlators: with quench operator $(I + iA)/\sqrt{2}$, measurements in the eigenbasis of B yield $\text{Im}[C(A, B, t)]$ [see Eq. (2)]. Step 2: Prepare the symmetric and asymmetric thermal states ρ_S, ρ_A [see Eq. (16)] and use the quench operator $(P + A)/\sqrt{2}$; $\text{Re}[C(A, B, t)]$ is then obtained from a linear combination of measurements. Step 3: Perform signal analysis to reconstruct the Green's function.

tation value of this time-dependent measurement as the *quench function*.

For systems with parity symmetry, we construct two quench operators: $(I + iA)/\sqrt{2}$ and $(P + A)/\sqrt{2}$. The former yields $\text{Im}[C(A, B, t)]$, and the latter gives $\text{Re}[C(PA, B, t)]$, where $C(A, B, t)$ is the *two-point time correlator*. If the initial state satisfies $P\rho = \rho$, these components already determine $C(A, B, t)$. For finite-temperature thermal states, this condition generally fails, so we instead apply TQS to the symmetric and asymmetric thermal states, which are the equilibrium states of $(H \pm HP)/2$. We show that $\text{Re}[C(A, B, t)]$ can be extracted as linear combinations of the quench functions, enabling reconstruction of the Green's function. Additionally, we show that the same technique extends naturally to the *out-of-time-order correlator* (OTOC).

Comparison to other ancilla-free methods—For systems with parity symmetry, Green's functions can also be estimated without ancilla qubits using the linear-response framework [23–25] or quantum imaginary-time evolution [32–34]. However, our TQS approach offers several distinct advantages: i) it requires no simulation of time-dependent Hamiltonians, significantly reducing experimental complexity; ii) it yields exact, non-perturbative recovery of correlators, hence significantly limiting sources of error; and iii) unlike imaginary-time methods, which perturb the state via $e^{-\tau O}$ using complicated techniques like Trotterization or dissipative evolution, it uses considerably simpler operations.

Green's function—We begin by clarifying the relationship between Green's functions and two-point time correlators. Consider a target Hamiltonian H with the spectral decomposition $H = \sum_{n=0}^{D-1} E_n |n\rangle \langle n|$. Let O_a and O_b be two linear operators. In many-body physics, the two-point time correlator is defined as

$$C(O_a, O_b, t_1, t_2) := \text{Tr}[\rho O_a(t_1) O_b(t_2)], \quad (1)$$

where $O(t) := e^{iHt} O e^{-iHt}$. If $[\rho, H] = 0$, the correlator simplifies to $C(O_a, O_b, t_2 - t_1)$, expressed as

$$C(O_a, O_b, t) := \text{Tr}[\rho O_a O_b(t)]. \quad (2)$$

Using the spectral decomposition of H , the correlator can be written as

$$\sum_{m,n} \langle n | O_b | m \rangle \langle m | \rho O_a | n \rangle e^{i(E_m - E_n)t}. \quad (3)$$

The (Lehmann representation of) Green's function is defined by the frequencies and amplitudes of the two-point time correlator [35]:

$$G(z) := \sum_{m,n} \frac{\langle n | O_b | m \rangle \langle m | \rho O_a | n \rangle}{z - E_m + E_n}. \quad (4)$$

In fermionic systems, the operators O_a and O_b are typically linear combinations of $\{c_i, c_i^\dagger\}_i$, where $\{c_i\}_i$ denotes the set of fermionic annihilation operators. Suppose $O_a = \sum_i a_i c_i$ and $O_b = \sum_i b_i c_i^\dagger$. By linearity, we have

$$C(O_a, O_b, t) = \sum_{i,i'} a_i b_{i'} C(c_i, c_{i'}^\dagger, t). \quad (5)$$

Thus, computing all $C(c_i, c_{i'}^\dagger, t)$ enables the recovery of any Green's function of this form. Using the Jordan-Wigner transformation, a fermionic annihilation operator can be expressed as $c_i = A + iB$, where A and B are Pauli operators that anticommute with each other. If $c_i = A_0 + iB_0$ and $c_{i'} = A_1 + iB_1$, then $C(c_i, c_{i'}^\dagger, t)$ decomposes into

$$\begin{aligned} & C(A_0, A_1, t) + C(B_0, B_1, t) \\ & - iC(A_0, B_1, t) + iC(B_0, A_1, t). \end{aligned} \quad (6)$$

Consequently, the problem reduces to estimating a general two-point time correlator of the form $C(A, B, t)$, which is the primary focus of this paper.

Without ancillas, directly measuring complex amplitudes such as $C(A, B, t)$ is nontrivial. Here, we propose a QS-based ancilla-free protocol by exploiting parity symmetry.

Parity symmetry—If there exists a parity operator P such that $[H, P] = 0$, then we say the system has parity symmetry. This seemingly strong condition is actually common in typical quantum systems. For example, the Heisenberg model

$$H_{\text{XXZ}} = J_X \left(\sum_{n=0}^{N-2} X_n X_{n+1} + Y_n Y_{n+1} \right) + J_Z \sum_{n=0}^{N-2} Z_n Z_{n+1} + h \sum_{n=0}^{N-1} Z_n. \quad (7)$$

commutes with $P := \prod_{j=0}^{N-1} Z_j$. As another example, consider the general Fermi-Hubbard model

$$H_{\text{FH}} = - \sum_{j=0}^{N-1} \sum_{\sigma=\uparrow,\downarrow} \left(c_{j,\sigma}^\dagger c_{j+1,\sigma} + c_{j+1,\sigma}^\dagger c_{j,\sigma} \right) + h_U \sum_{j=0}^{N-1} n_{j,\uparrow} n_{j,\downarrow}. \quad (8)$$

Its parity operator is the product of all the Majorana operators: $P = \prod_{j,\sigma} \exp(i\pi n_{j,\sigma})$. Under the Jordan-Wigner representation, it can be mapped to a spin system on $2N$ lattices, and the parity operator becomes $P = \prod_{j=0}^{2N-1} Z_j$. In the next lemma, we first prove that the parity of an eigenstate can be defined properly; see Sec. S3 A in Supplemental Material (SM) for the proof.

Lemma 1. *Suppose H is a Hermitian operator commuting with P . Then there exists an eigenstate decomposition of $H = \sum_n E_n |n\rangle\langle n|$, such that $\langle n|P|n\rangle \in \{\pm 1\}$.*

Define $p_n := \langle n|P|n\rangle$ for all n . If $p_n = 1$, then we say the eigenstate $|n\rangle$ has even parity; otherwise, it has odd parity. We then observe the following fact; see SM Sec. S3 B for the proof.

Lemma 2. *Suppose $[H, P] = \{P, A\} = 0$ and $|m\rangle, |n\rangle$ are two eigenstate of H . Then $\langle n|A|m\rangle \neq 0$ implies that $|m\rangle, |n\rangle$ have different parity.*

In the remaining part of the paper, we assume the observables of interest anticommute with P , and P is a traceless Hermitian operator with $P^2 = I$.

Tailored quench spectroscopy for time correlators—Using the QS method [12, 13], we can compute the two-point time correlators when the initial state is an eigenstate, and the Hamiltonian and observables satisfy the parity symmetry conditions. The procedure is illustrated in Fig. 1. Suppose ρ is a quantum state satisfying $[\rho, H] = 0$. We define the

quench function as the expectation value of the measurement outcomes:

$$Q(\rho, K, M) := \text{Tr}(K\rho K^\dagger M). \quad (9)$$

Let A be a traceless Hermitian operator with $A^2 = I$. Suppose $K = e^{i\pi A/4} = (I + iA)/\sqrt{2}$. Then for any ρ, t, M , we have [36]

$$\begin{aligned} \text{Im}[C(A, B, t)] &= Q(\rho, e^{i\pi A/4}, B(t)) \\ &\quad - \frac{1}{2}Q(\rho, A, B(t)) - \frac{1}{2}Q(\rho, I, B(t)). \end{aligned} \quad (10)$$

Note that the parity symmetry condition is not required up to this step.

Suppose $K = (P + A)/\sqrt{2}$, which is the product of two Pauli rotations:

$$\frac{P + A}{\sqrt{2}} = P \exp \left[i \frac{\pi}{4} (-iPA) \right]. \quad (11)$$

Then in conjunction with the fact that $[\rho, P] = 0$, we obtain

$$\begin{aligned} \text{Re}[C(PA, B, t)] &= Q[\rho, (P + A)/\sqrt{2}, B(t)] \\ &\quad - \frac{1}{2}Q(\rho, P, B(t)) - \frac{1}{2}Q(\rho, A, B(t)). \end{aligned} \quad (12)$$

Together, the protocol based on $K = (I + iA)/\sqrt{2}$ and $K = (P + A)/\sqrt{2}$ is called *tailored quench spectroscopy* (TQS).

When $\rho = |\Psi\rangle\langle\Psi|$ is an eigenstate of H , we have the following result; see SM Sec. S3 C for the proof.

Theorem 1. *Suppose H is a Hamiltonian that commutes with P , and A and B are two Hermitian operators satisfying $\{A, P\} = \{B, P\} = 0$. If $\rho = |\Psi\rangle\langle\Psi|$ is an eigenstate of H with $P|\Psi\rangle = p|\Psi\rangle, p \in \{\pm 1\}$, then $C(A, B, t)$ equals to*

$$pQ \left(\rho, \frac{P + A}{\sqrt{2}}, B(t) \right) + iQ \left(\rho, \frac{I + iA}{\sqrt{2}}, B(t) \right). \quad (13)$$

For the case when the initial state is a finite-temperature thermal state (also called a Gibbs state) $\rho_\beta := e^{-\beta H}/\mathcal{Z}$, where β is the inverse temperature and $\mathcal{Z} := \text{Tr}(e^{-\beta H})$, we do not have the condition $\rho P = \rho$ in general. To address this issue, we introduce the symmetric and asymmetric thermal states.

Symmetric (Asymmetric) thermal state—Decompose the full Hamiltonian into $H = H_A + H_S$, where

$$H_S := \frac{H + HP}{2} = \sum_{n \in \mathcal{N}_S} E_n |n\rangle\langle n|, \quad (14)$$

$$H_A := \frac{H - HP}{2} = \sum_{n \in \mathcal{N}_A} E_n |n\rangle\langle n|, \quad (15)$$

where $\mathcal{N}_S := \{n : p_n = 1\}$ is the Hilbert spaces with even symmetry and $\mathcal{N}_A := \{n : p_n = -1\}$ with odd

symmetry. We define the *symmetric thermal state* ρ_S as the thermal state of H_S :

$$\rho_S := \frac{e^{-\beta H_S}}{\text{Tr}(e^{-\beta H_S})}, \quad (16)$$

and similarly the *asymmetric thermal state* ρ_A as the thermal state of H_A . Let $\mathcal{Z}_S := \sum_{n \in \mathcal{N}_S} e^{-\beta E_n}$ and $\mathcal{Z}_A := \sum_{n \in \mathcal{N}_A} e^{-\beta E_n}$. Note that

$$\text{Tr}(\rho_S P) = \frac{\mathcal{Z}_S - |\mathcal{N}_A|}{\mathcal{Z}_S + |\mathcal{N}_A|}, \quad (17)$$

$$\text{Tr}(\rho_A P) = \frac{|\mathcal{N}_S| - \mathcal{Z}_A}{|\mathcal{N}_S| + \mathcal{Z}_A}. \quad (18)$$

Together with the other two conditions

$$|\mathcal{N}_S| + |\mathcal{N}_A| = d, \quad \text{Tr}(\rho P) = \frac{\mathcal{Z}_S - \mathcal{Z}_A}{\mathcal{Z}_S + \mathcal{Z}_A}, \quad (19)$$

we can solve for the following four parameters: $\mathcal{Z}_S, \mathcal{Z}_A, |\mathcal{N}_S|, |\mathcal{N}_A|$.

By applying TQS, we can estimate the real component of $C(A, B, t)$ efficiently by using a quantum computer, as shown in the following theorem; see SM Sec. S3 D for the proof.

Theorem 2. Suppose H is a Hamiltonian that commutes with P , and A and B are two Hermitian operators satisfying $\{A, P\} = \{B, P\} = 0$. Let $\rho_\beta, \rho_S, \rho_A$ be the thermal states of H, H_S, H_A at inverse temperature β . Then we have

$$\frac{|\mathcal{N}_S|}{|\mathcal{N}_A|} = \frac{1 + \text{Tr}(\rho_A P)}{1 - \text{Tr}(\rho_A P)} \frac{1 + \text{Tr}(\rho_S P)}{1 - \text{Tr}(\rho_S P)} \frac{1 - \text{Tr}(\rho P)}{1 + \text{Tr}(\rho P)}. \quad (20)$$

If the initial state is ρ_β , we further have

$$\begin{aligned} \text{Re}[C(A, B, t)] &= \frac{\mathcal{Z}_S + |\mathcal{N}_A|}{\mathcal{Z}} Q\left(\rho_S, \frac{P + A}{\sqrt{2}}, B(t)\right) \\ &\quad - \frac{|\mathcal{N}_S| + \mathcal{Z}_A}{\mathcal{Z}} Q\left(\rho_A, \frac{P + A}{\sqrt{2}}, B(t)\right) \\ &\quad + \frac{1}{\mathcal{Z}} \text{Re}[\text{Tr}(AB(t))]. \end{aligned} \quad (21)$$

Note that the terms on the RHS can be directly measured on a quantum computer. In particular, $\text{Tr}(AB(t))$ can be estimated by setting $(I + A)/d$ as the initial state.

Although quantum thermal state preparation is not the focus of this work, we would like to point out a few possible options. For early or fully fault-tolerant quantum computers, one may employ recently developed quantum Gibbs sampling algorithms [37–40], in which the target Gibbs state can be prepared as the fixed point of an algorithmically constructed Lindbladian that can be efficiently simulated on a quantum computer. For near-term devices, one may consider [41].

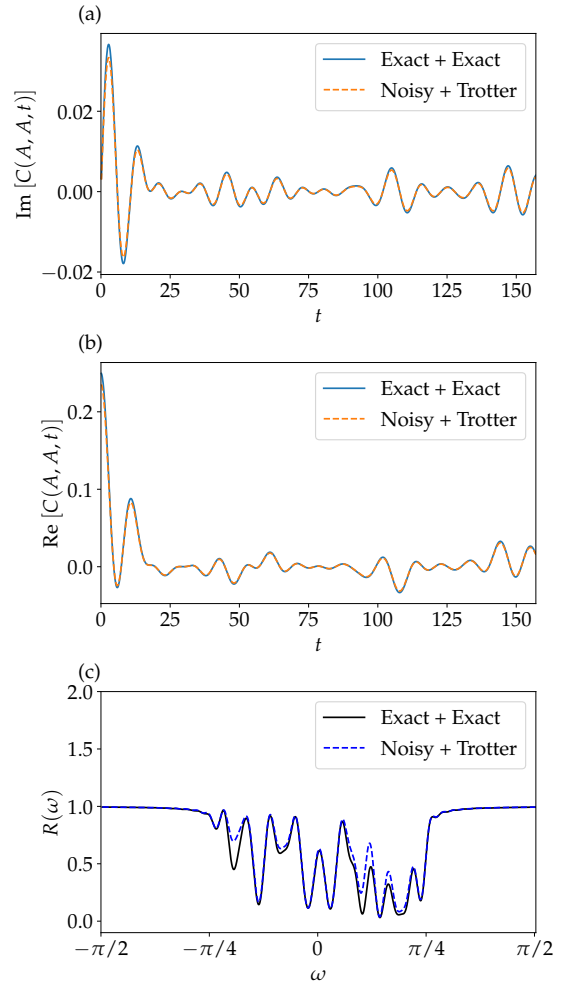


FIG. 2. Finite-temperature Green's function for the 2D Fermi–Hubbard model on a 2×3 lattice without periodic boundary conditions. The initial state is ρ_β with $\beta = 1$, and the interaction strength is $h_U = 6$. The observable is $A = B = (c_0 + c_0^\dagger)/2$. The system is evolved up to time 50π with a Trotter step of $\pi/20$. Noise of strength $\varepsilon = 0.1$ is introduced by adding an identical random perturbation ϱ at each time step. In the legend, the first “Exact” denotes an exact initial state, the second “Exact” denotes exact time evolution, “Noisy” corresponds to the perturbed initial state $\rho_\beta + \varepsilon\varrho$ after rescaling, and “Trotter” refers to simulation via TS decomposition. (a) Imaginary part of $C(A, A, t)$ as a function of time. (b) Real part of $C(A, A, t)$. (c) Comparison of the noise-space correlation function $R(\omega)$ [see SM Eq. (S29)] for $\omega \in [-\pi/2, \pi/2]$. Due to the denoising effect of the MULTiple SIgnal Classification (MUSIC) algorithm [42] we use, the positions of the local minima of $R(\omega)$ remain largely unchanged in the noisy model.

The pseudocode for all the protocols can be found in SM Sec. S5.

Numerical simulation and error analysis—In this section we conduct extensive numerical experiments and demonstrate that our algorithm is robust against

Trotter error and state preparation and measurement (SPAM) error.

The standard ancilla-free method for simulating quantum dynamics is the Trotter-Suzuki (TS) formula [43, 44]. A time-independent Hamiltonian can be simulated by

$$U_{\text{TS}}(t) := \left[\prod_{\gamma=1}^{\Gamma} \exp(-iH_{\gamma}t/N_T) \right]^{N_T}, \quad (22)$$

where $H = \sum_{\gamma} H_{\gamma}$, and each H_{γ} only contains mutually commuting Pauli operators. Here N_T is the number of layers in the quantum circuit, which is directly related to the circuit complexity of the algorithm. Typically, the norm distance error of the formula scales as $\mathcal{O}(\|H\|tN_T^{-2})$. Higher order Trotter-Suzuki formulas can reduce the error scaling to $\mathcal{O}(\|H\|tN_T^{-1})$. Note that because U_{TS} commutes with P , the effective Hamiltonian of U_{TS} also has parity symmetry, hence the previous conclusions still apply.

There are two main sources of noise that we consider: the inaccuracy of the initial state preparation, and the random fluctuation in measurements. More specifically, we can do the following: First generate a traceless Hermitian matrix E such that for each entry $a + ib$, a and b are two random numbers drawn from $\mathcal{N}(0, 1)$. Then normalize E as \tilde{E} with $\|\tilde{E}\|_1 = 1$. Let $\varrho := e^{\tilde{E}}/\text{Tr}(e^{\tilde{E}})$. Choose a noise strength parameter $\varepsilon \in [0, 1]$ and add $\varepsilon\varrho$ to the initial state ρ . Finally, renormalize the perturbed matrix to trace 1 as $\tilde{\rho}$, which approximately satisfies $\|\rho - \tilde{\rho}\|_1 \approx \varepsilon$.

In Fig. 2, we demonstrate robust numerical results for a rescaled Fermi-Hubbard model (FHM) with spectral norm π on a 2×3 lattice without periodic boundary conditions. There are totally 12 different single-particle states labelled as:

$$(x, y, \uparrow) : 6x + 2y, \quad (x, y, \downarrow) : 6x + 2y + 1, \quad (23)$$

where $x = 0, 1$; $y = 0, 1, 2$ labels the position on the lattice. In the TS formula, the rescaled Hamiltonian can be decomposed into four commuting layers:

$$\begin{aligned} T_1 &= -\gamma \sum_{j=0,1,6,7} (c_j^{\dagger}c_{j+2} + c_{j+2}^{\dagger}c_j), \\ T_2 &= -\gamma \sum_{j=2,3,8,9} (c_j^{\dagger}c_{j+2} + c_{j+2}^{\dagger}c_j), \\ T_3 &= -\gamma \sum_{j=0}^5 (c_j^{\dagger}c_{j+6} + c_{j+6}^{\dagger}c_j), \\ T_4 &= -\gamma h_U \sum_{j=0}^5 n_{2j}n_{2j+1}, \end{aligned} \quad (24)$$

where $\gamma := \pi/\|H_{\text{FH}}\|$.

Additional numerical results can be found in SM Sec. S6, where we consider the finite-temperature

Green's function for FHM with weak coupling as well as the zero-temperature (i.e., ground-state) Green's functions under strong and weak couplings. For zero temperature, our numerical result also shows that the excitation spectrum $\{E_n - E_0 : |\langle n|A|0\rangle|^2 > 0.01\}$ matches exactly with the local minima of the noise-space correlation function, which further confirms the accuracy and robustness of our algorithm. Note that for finite temperature, since the minimal energy gap could be extremely small, and the MUSIC algorithm needs total evolution time $\mathcal{O}(\Delta E^{-1})$ to distinguish two frequencies with gap ΔE , it is numerically more challenging to demonstrate such exact match. In SM Sec. S7, we further demonstrate the versatility of our protocol by extending it to OTOC.

Conclusion and outlook—In this work, we have presented a novel TQS protocol for computing two-point time correlators and reconstructing thermal Green's functions of parity-symmetric systems without ancillas, relying solely on native time evolution and measurements. The method is exact, resilient to noise, and broadly applicable to both digital and analog quantum simulators. Our construction also extends naturally to other correlators, such as OTOCs, highlighting its versatility.

Looking ahead, several exciting directions emerge. Can this framework be generalized to probe non-linear or non-Hermitian responses [45, 46]? Could it be extended to n -time quantum correlators, enabling access to richer dynamical information? Finally, is the parity-symmetry condition fundamental, or can it be relaxed through symmetrization channel $\mathcal{S}(\rho) := (\rho + P\rho P)/2$? Addressing these questions would further expand the reach of ancilla-free quantum protocols, paving the way toward experimentally practical studies of strongly correlated matter on near-term and early fault-tolerant quantum devices.

Acknowledgement—C.Y. acknowledges support from the National Key Research and Development Program of China (Grant No. 2022YFA1404204), Shanghai Municipal Science and Technology Major Project (Grant No. 2019SHZDZX01), and National Natural Science Foundation of China (Grant No. 92165109). C.Z. acknowledges support from the Faculté des sciences and Institut quantique at Université de Sherbrooke, as well as from the Institut transdisciplinaire d'information quantique (INTIQU), a strategic cluster funded by the Fonds de recherche du Québec – Nature et technologies. We sincerely thank Dr. Mario Motta for his careful reading of our draft and for the numerous insightful comments he provided.

Data availability—The data that support the findings of this article are openly available [47].

[1] A. Altland and B. D. Simons, *Condensed matter field theory* (Cambridge University Press, Cambridge, UK, 2010).

[2] H. Zhang, T. Pincelli, C. Jozwiak, T. Kondo, R. Ernststorfer, T. Sato, and S. Zhou, Angle-resolved photoemission spectroscopy, *Nat. Rev. Methods Primers* **2**, 54 (2022).

[3] L. J. P. Ament, M. van Veenendaal, T. P. Devereaux, J. P. Hill, and J. van den Brink, Resonant inelastic X-ray scattering studies of elementary excitations, *Rev. Mod. Phys.* **83**, 705 (2011).

[4] D. Zgid and G. K. Chan, Dynamical mean-field theory from a quantum chemical perspective, *J. Chem. Phys.* **134**, 10.1063/1.3556707 (2011).

[5] V. Viswanath and G. Müller, *The recursion method: application to many body dynamics*, Vol. 23 (Springer Science & Business Media, Berlin, Germeney, 1994).

[6] W. M. Foulkes, L. Mitas, R. Needs, and G. Rajagopal, Quantum Monte Carlo simulations of solids, *Rev. Mod. Phys.* **73**, 33 (2001).

[7] G. Vidal, Efficient simulation of one-dimensional quantum many-body systems, *Phys. Rev. Lett.* **93**, 040502 (2004).

[8] B. Bauer, D. Wecker, A. J. Millis, M. B. Hastings, and M. Troyer, Hybrid quantum-classical approach to correlated materials, *Phys. Rev. X* **6**, 031045 (2016).

[9] I. Loaiza, D. Motlagh, K. Hejazi, M. S. Zini, A. Delgado, and J. M. Arrazola, Nonlinear spectroscopy via generalized quantum phase estimation, *Quantum* **9**, 1822 (2025).

[10] J. S. Pedernales, R. Di Candia, I. L. Egusquiza, J. Casanova, and E. Solano, Efficient quantum algorithm for computing n -time correlation functions, *Phys. Rev. Lett.* **113**, 020505 (2014).

[11] M. Knap, A. Kantian, T. Giamarchi, I. Bloch, M. D. Lukin, and E. Demler, Probing real-space and time-resolved correlation functions with many-body Ramsey interferometry, *Phys. Rev. Lett.* **111**, 147205 (2013).

[12] L. Villa, J. Despres, and L. Sanchez-Palencia, Unraveling the excitation spectrum of many-body systems from quantum quenches, *Phys. Rev. A* **100**, 063632 (2019).

[13] L. Villa, *Out-of-equilibrium dynamics and quench spectroscopy of ultracold many-body quantum systems*, Ph.D. thesis, Institut Polytechnique de Paris (2021).

[14] Y. Yang, Y. Li, X. Xu, and X. Yuan, Resource-efficient quantum-classical hybrid algorithm for energy gap evaluation, *Phys. Rev. A* **109**, 052416 (2024).

[15] H. Chen, M. Nusspickel, J. Tilly, and G. H. Booth, Variational quantum eigensolver for dynamic correlation functions, *Phys. Rev. A* **104**, 032405 (2021).

[16] K. Huang, X. Cai, H. Li, Z.-Y. Ge, R. Hou, H. Li, T. Liu, Y. Shi, C. Chen, D. Zheng, *et al.*, Variational quantum computation of molecular linear response properties on a superconducting quantum processor, *J. Phys. Chem. Lett.* **13**, 9114 (2022).

[17] J. Sun, L. Vilchez-Estevez, V. Vedral, A. T. Boothroyd, and M. Kim, Probing spectral features of quantum many-body systems with quantum simulators, *Nat. Commun.* **16**, 1 (2025).

[18] E. Cruz, D. S. Wild, M. C. Bañuls, and J. I. Cirac, Quantum simulation of dynamical response functions of equilibrium states, arXiv:2505.05411.

[19] M. L. Baez, M. Goihl, J. Haferkamp, J. Bermejo-Vega, M. Gluza, and J. Eisert, Dynamical structure factors of dynamical quantum simulators, *Proc. Natl. Acad. Sci. U. S. A.* **117**, 26123 (2020).

[20] D. Cruz and D. Magano, Superresolution of Green's functions on noisy quantum computers, *Phys. Rev. A* **108**, 012618 (2023).

[21] D. Dhawan, D. Zgid, and M. Motta, Quantum algorithm for imaginary-time Green's functions, *J. Chem. Theory Comput.* **20**, 4629 (2024), pMID: 38761142, <https://doi.org/10.1021/acs.jctc.4c00241>.

[22] B. Gauthier, P. Rosenberg, A. Foley, and M. Charlebois, Occupation-number quantum-subspace-expansion approach to computing the single-particle Green function: An opportunity for noise filtering, *Phys. Rev. A* **110**, 032624 (2024).

[23] E. Kökcü, H. A. Labib, J. Freericks, and A. F. Kemper, A linear response framework for quantum simulation of bosonic and fermionic correlation functions, *Nat. Commun.* **15**, 3881 (2024).

[24] S. Piccinelli, F. Tacchino, I. Tavernelli, and G. Carleo, Efficient calculation of green's functions on quantum computers via simultaneous circuit perturbation (2025), arXiv:2505.05563 [quant-ph].

[25] G. Bishop, D. Bagrets, and F. K. Wilhelm, Quantum algorithm for Green's-function measurements in the Fermi-Hubbard model, *Phys. Rev. A* **111**, 062610 (2025).

[26] Y. Shen, A. Buzali, H.-Y. Hu, K. Klymko, D. Camps, S. F. Yelin, and R. V. Beeumen, Efficient measurement-driven eigenenergy estimation with classical shadows (2024), arXiv:2409.13691 [quant-ph].

[27] G. Greene-Diniz, D. Z. Manrique, K. Yamamoto, E. Plekhanov, N. Fitzpatrick, M. Krompiec, R. Sakuma, and D. M. Ramo, Quantum computed Green's functions using a cumulant expansion of the Lanczos method, *Quantum* **8**, 1383 (2024).

[28] R. Irmejs and R. A. Santos, Approximating dynamical correlation functions with constant depth quantum circuits, *Quantum* **9**, 1639 (2025).

[29] D. Aharonov, V. Jones, and Z. Landau, A polynomial quantum algorithm for approximating the jones polynomial (2006), arXiv:quant-ph/0511096 [quant-ph].

[30] J. Preskill, Quantum computing in the NISQ era and beyond, *Quantum* **2**, 79 (2018).

[31] A. Katabarwa, K. Gratsea, A. Caesura, and P. D. Johnson, Early fault-tolerant quantum computing, *PRX Quantum* **5**, 020101 (2024).

[32] M. Motta, C. Sun, A. T. Tan, M. J. O'Rourke, E. Ye, A. J. Minnich, F. G. Brandao, and G. K.-L. Chan, Determining eigenstates and thermal states on a quantum computer using quantum imaginary time evolution, *Nat. Phys.* **16**, 205 (2020).

[33] Y. Yang, A. Christianen, M. C. Bañuls, D. S. Wild, and J. I. Cirac, Phase-sensitive quantum measurement without controlled operations, *Phys. Rev. Lett.* **132**, 220601 (2024).

[34] X. Wang, L. Xiong, X. Cai, and X. Yuan, Computing n -time correlation functions without ancilla qubits (2025), arXiv:2504.12975 [quant-ph].

[35] M. M. Odashima, B. G. Prado, and E. Vernek, Pedagogical introduction to equilibrium Green's functions: condensed-matter examples with numerical implementations, *Revista Brasileira de Ensino de Física* **39**, 10.1590/1806-9126-RBEF-2016-0087 (2016).

[36] L. Vilchez-Estevez, R. A. Santos, S. Y. Wang, and F. M. Gambetta, Extracting the spin excitation spectrum of a fermionic system using a quantum processor, *Phys. Rev. B* **112**, 045143 (2025).

[37] C.-F. Chen, M. J. Kastoryano, F. G. S. L. Brandão, and A. Gilyén, Quantum thermal state preparation (2023), arXiv:2303.18224 [quant-ph].

[38] Y. Tong and Y. Zhan, Fast mixing of weakly interacting fermionic systems at any temperature, *PRX Quantum* **6**, 030301 (2025).

[39] D. Hahn, R. Sweke, A. Deshpande, and O. Shtanko, Efficient quantum Gibbs sampling with local circuits (2025), arXiv:2506.04321 [quant-ph].

[40] Z. Ding, Y. Zhan, J. Preskill, and L. Lin, End-to-end efficient quantum thermal and ground state preparation made simple (2025), arXiv:2508.05703 [quant-ph].

[41] J. Lloyd and D. A. Abanin, Quantum thermal state preparation for near-term quantum processors (2025), arXiv:2506.21318 [quant-ph].

[42] W. Liao and A. Fannjiang, MUSIC for single-snapshot spectral estimation: Stability and super-resolution, *Appl. Comput. Harmon. Anal.* **40**, 33 (2016).

[43] A. M. Childs and Y. Su, Nearly optimal lattice simulation by product formulas, *Phys. Rev. Lett.* **123**, 050503 (2019).

[44] A. M. Childs, Y. Su, M. C. Tran, N. Wiebe, and S. Zhu, Theory of Trotter error with commutator scaling, *Phys. Rev. X* **11**, 011020 (2021).

[45] L. Pan, X. Chen, Y. Chen, and H. Zhai, Non-Hermitian linear response theory, *Nat. Phys.* **16**, 767 (2020).

[46] K. T. Geier and P. Hauke, From non-Hermitian linear response to dynamical correlations and fluctuation-dissipation relations in quantum many-body systems, *PRX Quantum* **3**, 030308 (2022).

[47] <https://github.com/CYI1995/TailoredQuenchSpectroscopy> (2025).

[48] K. Mitarai and K. Fujii, Methodology for replacing indirect measurements with direct measurements, *Phys. Rev. Res.* **1**, 013006 (2019).

[49] A. Zhao, N. C. Rubin, and A. Miyake, Fermionic partial tomography via classical shadows, *Phys. Rev. Lett.* **127**, 110504 (2021).

[50] C. L. Cortes and S. K. Gray, Quantum krylov subspace algorithms for ground- and excited-state energy estimation, *Phys. Rev. A* **105**, 022417 (2022).

[51] K. Hashimoto, K. Murata, and R. Yoshii, Out-of-time-order correlators in quantum mechanics, *J. High Energy Phys.* **2017** (10), 1.

[52] I. García-Mata, R. Jalabert, and D. Wisniacki, Out-of-time-order correlations and quantum chaos, *Scholarpedia* **18**, 55237 (2023).

Ancilla-Free Quantum Protocol for Thermal Green's Functions: Supplemental Material

CONTENTS

S1. Background	1
A. Many-Body Green's Function	1
B. Jordan-Wigner Transformation	2
S2. Related Work	2
S3. Proof of Main Results	3
A. Proof of Lemma 1	3
B. Proof of Lemma 2	4
C. Proof of Theorem 1	4
D. Proof of Theorem 2	4
S4. Signal Analysis Algorithm	5
S5. Pseudocode for All Protocols	6
S6. Additional Numerical Results on Green's Functions	7
S7. Tailored Quench Spectroscopy Method for OTOC	8

S1. BACKGROUND

A. Many-Body Green's Function

In this section we give an overview of some basic facts about many-body Green's function in condensed matter physics. Suppose H is a Hamiltonian with a non-degenerate ground state and has eigendecomposition $H = \sum_{n=0}^{d-1} E_n |n\rangle\langle n|$. Let A, B be two linear operators. The many-body Green's function at zero-temperature is defined as:

$$G(z) := \langle 0 | A(z - H + E_0)^{-1} B | 0 \rangle = \sum_n \frac{\langle 0 | A | n \rangle \langle n | B | 0 \rangle}{z - E_n + E_0}, \quad \text{Im}(z) > 0. \quad (\text{S1})$$

Note that for all ζ with $\text{Re}(\zeta) > 0$, we have $\int_0^\infty e^{-\zeta t} dt = \zeta^{-1}$. In conjunction with the fact that

$$C(A, B, -t) = \sum_n \langle 0 | A | n \rangle \langle n | e^{-iHt} B e^{iHt} | 0 \rangle = \sum_n \langle 0 | A | n \rangle \langle n | B | 0 \rangle e^{i(E_0 - E_n)t}, \quad (\text{S2})$$

we obtain

$$\int_0^\infty e^{izt} e^{i(E_0 - E_n)t} dt = \int_0^\infty e^{i(z - E_n + E_0)t} dt = \frac{1}{z - E_n + E_0}, \quad (\text{S3})$$

$$\int_0^\infty e^{izt} C(A, B, -t) dt = G(z). \quad (\text{S4})$$

Let $z = \omega + i\eta$ with $\omega \in \mathbb{R}, \eta \in \mathbb{R}^+$. Then we have

$$G(z) = G(\omega + i\eta) = \sum_n \langle 0 | A_1^\dagger | n \rangle \langle n | A_2 | 0 \rangle \frac{(\omega - E_n + E_0) - i\eta}{(\omega - E_n + E_0)^2 + \eta^2}. \quad (\text{S5})$$

Let $\eta > 0$ be a constant, then

$$\begin{aligned} S(\omega, \eta) &:= -2\text{Im}[G(\omega + i\eta)] = \sum_n \langle 0 | A_1^\dagger | n \rangle \langle n | A_2 | 0 \rangle \frac{2\eta}{(\omega - E_n + E_0)^2 + \eta^2}, \\ \int_{-\infty}^{\infty} \frac{d\omega}{2\pi} \frac{S(\omega, \eta)}{z - \omega} &= \sum_n \langle 0 | A_1^\dagger | n \rangle \langle n | A_2 | 0 \rangle \int_{-\infty}^{\infty} \frac{d\omega}{2\pi} \frac{2\eta}{(\omega - E_n + E_0)^2 + \eta^2} \frac{1}{z - \omega}. \end{aligned} \quad (\text{S6})$$

Let $\Delta E_n = E_n - E_0$, then

$$\begin{aligned} \int_{-\infty}^{\infty} \frac{d\omega}{2\pi} \frac{2\eta}{(\omega - \Delta E_n)^2 + \eta^2} \frac{1}{z - \omega} &= \int_{-\infty}^{\infty} \frac{d\omega}{2\pi} \frac{2\eta}{\omega^2 + \eta^2} \frac{1}{z - \omega - \Delta E_n} \\ &= \frac{1}{\pi} \int_{-\infty}^{\infty} \frac{1}{z - \omega - \Delta E_n} d\arctan(\omega/\eta) \\ &= \frac{1}{\pi} \int_{-\pi/2}^{\pi/2} \frac{1}{z - \eta \tan \theta - \Delta E_n} d\theta \\ &\xrightarrow{\eta \rightarrow 0^+} \frac{1}{z - \Delta E_n}. \end{aligned} \quad (\text{S7})$$

Therefore,

$$\int_{-\infty}^{\infty} \frac{d\omega'}{2\pi} \frac{S(\omega', 0^+)}{\omega + i0^+ - \omega'} = G(\omega + i0^+) = \sum_n \frac{\langle 0 | A_1^\dagger | n \rangle \langle n | A_2 | 0 \rangle}{\omega - (E_n - E_0)}. \quad (\text{S8})$$

Moreover, it is direct to observe that

$$S(\omega') := \lim_{\eta \rightarrow 0^+} S(\omega', \eta) = 2\pi \sum_n \langle 0 | A_1^\dagger | n \rangle \langle n | A_2 | 0 \rangle \delta(\omega' - (E_n - E_0)), \quad (\text{S9})$$

which is termed as the *spectrum function* and is determined by the imaginary part of the Green's function.

B. Jordan-Wigner Transformation

Jordan-Wigner transformation can be used to map fermionic operators into Pauli strings. Consider a fermionic system with N sites and each site is further characterized by spin up or spin down, then the system has totally $J = 2N$ number of single-particle states. The standard Jordan-Wigner transformation writes

$$c_j = \left(\prod_{n=0}^{j-1} Z_n \right) \sigma_j^-, \quad \sigma_j^\pm = \frac{X_j \pm iY_j}{2}. \quad (\text{S10})$$

It is easy to show the following relations:

$$\begin{aligned} c_j c_j^\dagger &= \frac{1 - Z_j}{2}, \quad n_j := c_j^\dagger c_j = \frac{1 + Z_j}{2}, \\ c_j c_{j+1}^\dagger &= \sigma_j^- \sigma_{j+1}^+, \quad c_{j+1}^\dagger c_j = -\sigma_j^- \sigma_{j+1}^+, \\ c_j c_{j+1}^\dagger + c_{j+1} c_j^\dagger &= \frac{X_j X_{j+1} + Y_j Y_{j+1}}{2}. \end{aligned} \quad (\text{S11})$$

Note that $[c_i c_j^\dagger, c_k c_l^\dagger] = 0$ iff $(i, j) \neq (k, l)$, which is useful in the Trotter-Suzuki simulation of fermionic systems.

S2. RELATED WORK

We give an overview of several related methods for estimating Green's function, highlighting their key features, advantages, and limitations.

Quench Spectroscopy (QS) Method [11, 12, 14, 17, 19]. This widely adopted protocol, inspired by the Ramsey interferometer, probes dynamical response functions, as introduced in [11]. Early studies, such as [12], assumed the system exhibits translation symmetry, meaning that the Hamiltonian commutes with a translation operator \hat{T} . The quench operator is defined as $e^{i\hat{T}x}$, and the QS function is expressed as a function of x and t . These studies focused on fermionic correlation functions of the form $iC(A, B, t) - iC(B, A, t)$, which is equivalent to $\text{Im}[C(A, B, t)]$. Our work extends this method to bosonic correlation functions of the form $iC(A, B, t) + iC(B, A, t)$, substantially broadening its applicability.

Replacing indirect measurements with direct measurements [48]. Compared to our TQS approach, where we use the quench operator $(P + A)/\sqrt{2}$ to estimate $\text{Re}[C(A, B, t)]$, they do not assume parity symmetry and instead directly evaluate $\text{Tr}[(I + A)\rho(I + A)B(t)]/4$ via mid-circuit measurements. The procedure is as follows: first measure ρ in the eigenbasis of A . If the outcome corresponds to an eigenvalue $+1$, prepare the corresponding eigenstate, evolve it under e^{-iHt} , then measure it in the eigenbasis of B and record the outcome. If the outcome corresponds to -1 , record 0 . The overall measurement budget is comparable to that of TQS. However, the main drawback of this method is that after each measurement in the A -basis, one must prepare a different state, which is experimentally demanding. Moreover, mid-circuit measurements in current hardware are typically slow and noisy, requiring additional latency for classical feedforward and introducing crosstalk that can disturb other qubits. These practical limitations make the direct measurement approach less appealing compared to TQS in near-term devices.

Linear Response Framework [23–25]. This method leverages the deep connection between Green’s function and linear response theory. Instead of applying a quench operator before time evolution, a time-dependent perturbation is introduced to the Hamiltonian: $H(t) = H + \varepsilon A(t)$. The evolved state is measured at various times, with the time correlator appearing in the leading perturbation term of $\langle A(t) \rangle$. However, simulating a time-dependent Hamiltonian is typically more complex than a time-independent one. Moreover, the result is only an approximation of the true Green’s function due to higher-order perturbation effects. The method’s strength lies in its straightforward generalization to thermal state scenarios.

Quantum Imaginary Time Evolution [32–34]. This approach employs normalized quantum imaginary time evolution, mapping $|\Psi\rangle$ to $e^{-\tau O}|\Psi\rangle/\sqrt{\langle\Psi|e^{-2\tau O}|\Psi\rangle}$, implemented via Trotter-Suzuki formulas. Imaginary time evolution introduces a perturbation along the imaginary axis, $t \rightarrow t + i\tau$, to a real-valued time-dependent function. The n -time correlators are obtained by differentiating with respect to τ . This method is ancilla-free, but its accuracy is limited to the asymptotic limit $\tau \rightarrow 0$.

Direct Computation by Krylov Space Method [27, 28]. This approach uses a recursive analytical formula for the Green’s function, with coefficients determined by the target state ρ , observables A , and the Hamiltonian H_0 . These parameters can be estimated experimentally using standard shadow tomography [49]. Unlike other methods, this approach does not require simulating quantum dynamics. However, it suffers from high sample complexity, which scales with the dimension of the quantum system.

A related work [50] demonstrated how symmetries can be exploited to avoid the use of the Hadamard test for ground- and excited-state energy estimation. In that approach, the controlled time evolution, which is absent in the case of Green’s functions, is replaced by the preparation of a superposition of states belonging to two different symmetry sectors.

Multiple-Observable Method [26] can be used to estimate the time correlator without measuring the evolution of observables. Although it avoids controlled unitaries, it requires an additional ancilla qubit, and controlled quantum gates may be necessary during state preparation. Furthermore, achieving accurate estimations using Eq. (27) of [26] involves summing over a large number of energy levels, posing significant computational and experimental challenges.

S3. PROOF OF MAIN RESULTS

A. Proof of Lemma 1

Proof. For a system with parity symmetry, any non-degenerate eigenstate of H is also an eigenstate of P . Since P is a Hermitian operator with eigenvalues ± 1 , we have $P|n\rangle = p|n\rangle, p \in \{\pm 1\}$ for all non-degenerate n . If $p = 1$, we say the eigenstate has even parity; otherwise, it has odd parity. If the Hamiltonian has degeneracy, then we cannot associate the degenerate subspace with a unique parity. But the degenerate subspaces can still be decomposed according to the parity operator P . In particular, if $\Pi = \sum_{i=0}^{\chi-1} |v_i\rangle\langle v_i|$ is a maximal eigenspace projector of H with energy E , then $\{P|v_i\rangle\}_{i=0}^{\chi-1}$ is a vector basis of the image space of Π . Let $\mathcal{P}_{ij} := \langle v_j|P|v_i\rangle$ $i, j = 0, \dots, \chi - 1$. From the diagonalization of \mathcal{P} , we can decompose the image space

of Π into the $+1$ and -1 parity subspaces. This completes the proof of Lemma 1. \square

B. Proof of Lemma 2

Proof. Observe that

$$\langle n|A|m\rangle = -\langle n|PAP|m\rangle = -p_m p_n \langle n|A|m\rangle. \quad (\text{S12})$$

Hence, if $p_n p_m = 1$, then $\langle n|A|m\rangle = 0$. Conversely, if $\langle n|A|m\rangle \neq 0$, then $p_n p_m = -1$. This completes the proof of Lemma 2. \square

C. Proof of Theorem 1

Proof. Note that $\{B(t), P\} = 0$. For any state ρ that commutes with P , we have

$$\begin{aligned} Q(\rho, A, B(t)) &= \text{Tr}(A\rho AB(t)) \\ &= \text{Tr}(AP\rho PAB(t)) \\ &= \text{Tr}(PA\rho APB(t)) \\ &= -\text{Tr}(A\rho AB(t)) \\ &= -Q(\rho, A, B(t)). \end{aligned} \quad (\text{S13})$$

Hence, $Q(\rho, A, B(t)) = 0$. Similarly, $Q(\rho, I, B(t)) = Q(\rho, P, B(t)) = 0$. This confirms that

$$\text{Im}[C(A, B, t)] = Q(\rho, e^{i\pi A/4}, B(t)), \quad \text{Re}[C(PA, B, t)] = Q(\rho, Pe^{\pi PA/4}, B(t)). \quad (\text{S14})$$

If we set $\rho = |\Psi\rangle\langle\Psi|$, then $\rho P = p\rho$ with $p \in \{\pm 1\}$. Hence

$$C(PA, B, t) = \text{Tr}(\rho PAB(t)) = p\text{Tr}(\rho AB(t)) = pC(A, B, t), \quad (\text{S15})$$

which confirms

$$\text{Re}[C(A, B, t)] = p\text{Re}[C(PA, B, t)] = p\text{Re}\left[Q(\rho, Pe^{\pi PA/4}, B(t))\right]. \quad (\text{S16})$$

This completes the proof of Theorem 1. \square

D. Proof of Theorem 2

Proof. By definition,

$$\frac{\mathcal{Z}_S}{|\mathcal{N}_A|} = \frac{1 + \text{Tr}(\rho_S P)}{1 - \text{Tr}(\rho_S P)}, \quad \frac{\mathcal{Z}_A}{|\mathcal{N}_S|} = \frac{1 - \text{Tr}(\rho_A P)}{1 + \text{Tr}(\rho_A P)}, \quad \frac{\mathcal{Z}_S}{\mathcal{Z}_A} = \frac{1 + \text{Tr}(\rho P)}{1 - \text{Tr}(\rho P)}. \quad (\text{S17})$$

The three ratios together confirm Eq. (20).

Introduce

$$\lambda := \frac{d}{2[1 + \text{Tr}(\rho_A P)\text{Tr}(\rho_S P) - \text{Tr}(\rho P)\text{Tr}(\rho_A P) - \text{Tr}(\rho P)\text{Tr}(\rho_S P)]} \quad (\text{S18})$$

Then

$$\mathcal{N}_S = [1 + \text{Tr}(\rho_A P)][1 + \text{Tr}(\rho_S P)][1 - \text{Tr}(\rho P)]\lambda, \quad (\text{S19})$$

$$\mathcal{N}_A = [1 - \text{Tr}(\rho_A P)][1 - \text{Tr}(\rho_S P)][1 + \text{Tr}(\rho P)]\lambda, \quad (\text{S20})$$

$$\mathcal{Z}_S = [1 - \text{Tr}(\rho_A P)][1 + \text{Tr}(\rho_S P)][1 + \text{Tr}(\rho P)]\lambda, \quad (\text{S21})$$

$$\mathcal{Z}_A = [1 - \text{Tr}(\rho_A P)][1 + \text{Tr}(\rho_S P)][1 - \text{Tr}(\rho P)]\lambda, \quad (\text{S22})$$

$$\mathcal{Z} = 2[1 - \text{Tr}(\rho_A P)][1 + \text{Tr}(\rho_S P)]\lambda. \quad (\text{S23})$$

We have

$$\begin{aligned}\text{Tr}(\rho_S PAB(t)) &= \frac{\sum_{n \in \mathcal{N}_S} e^{-\beta E_n} \langle n | AB(t) | n \rangle - \sum_{n \in \mathcal{N}_A} \langle n | AB(t) | n \rangle}{|\mathcal{N}_A| + \mathcal{Z}_S}, \\ \text{Tr}(\rho_A PAB(t)) &= \frac{-\sum_{n \in \mathcal{N}_A} e^{-\beta E_n} \langle n | AB(t) | n \rangle + \sum_{n \in \mathcal{N}_S} \langle n | AB(t) | n \rangle}{|\mathcal{N}_S| + \mathcal{Z}_A}.\end{aligned}\quad (\text{S24})$$

A straightforward calculation then gives

$$\begin{aligned}(\mathcal{Z}_S + \mathcal{Z}_A) \text{Re}[\text{Tr}(\rho AB(t))] &= (|\mathcal{N}_A| + \mathcal{Z}_S) \text{Re}[\text{Tr}(\rho_S PAB(t))] \\ &\quad - (|\mathcal{N}_S| + \mathcal{Z}_A) \text{Re}[\text{Tr}(\rho_A PAB(t))] + \text{Re}[\text{Tr}(AB(t))].\end{aligned}\quad (\text{S25})$$

This completes the proof of Theorem 2. \square

S4. SIGNAL ANALYSIS ALGORITHM

We use MULTiple SIgnal Classification (MUSIC) algorithm [42] for signal analysis in our numerical test. Here we give a brief introduction of this method. Consider time-domain signals of the form

$$s_n = \sum_{k=1}^{\chi} c_k e^{-i f_k n}, \quad f_k \in [0, 2\pi], \quad n = 1, 2, \dots, 2N. \quad (\text{S26})$$

Construct the so-called Hankel matrix

$$M_{m,n} := s_{m+n}, \quad m, n \leq N. \quad (\text{S27})$$

Suppose $N \geq \chi$. Then M has rank at most χ . With singular value decomposition, we obtain $M = U \Sigma V^\top$, where the diagonal entries of Σ is arranged in the non-increasing order so that the last $N - \chi$ diagonal entries of Σ are 0. Define

$$a(f) := [e^{-i f n}]_{n=1}^N. \quad (\text{S28})$$

Note that $s_n = \sum_{k=1}^{\chi} c_k a(f_k)_n$. Hence, $\text{span}\{a(f_1), \dots, a(f_\chi)\} = \text{span}\{U_1, \dots, U_\chi\}$, where U_k is the k -th column of the matrix U . Set the first χ columns of U to 0. Then we get U_{null} , which satisfies $U_{\text{null}} a(f_k) = 0$ for all k . Introduce the noise-space correlation function

$$R(\omega) := \|U_{\text{null}} a(\omega)\|_2. \quad (\text{S29})$$

Then $\{f_k\}_{k=1}^{\chi}$ are the roots of $R(\omega) = 0$.

We have the following established result about the accuracy of MUSIC for noisy signals.

Theorem S1 (Corollary 1 in [42]). *Suppose $(s_n)_{n=1}^{2N}$ is a length-(2N) signal satisfying*

$$\min_{k_1 \neq k_2} |f_{k_1} - f_{k_2}| = \Omega(N^{-1}), \quad (\text{S30})$$

where s_n is of the form Eq. (S26), and $(e_n)_{n=1}^{2N}$ is 2N i.i.d. random parameters with variance σ^2 . Input noisy signal $(s_n + e_n)_{n=1}^{2N}$ to the MUSIC algorithm, and denote the new noise-space correlation function as $\tilde{R}(\omega)$. Then with high probability, we have

$$\max_{\omega} |\tilde{R}(\omega) - R(\omega)| = \mathcal{O}\left(\sigma N^{-1/2}\right). \quad (\text{S31})$$

Unfortunately, the result Eq. (S31) cannot be directly translated into an error bound on the accuracy of f_k . In the ideal case [see Remark 11 of [42]], the final accuracy can be improved to $\mathcal{O}(\sigma N^{-3/2})$.

S5. PSEUDOCODE FOR ALL PROTOCOLS

Algorithm 1 MUSIC

Input: Signal $(s_n)_{n=1}^{2N}$.

Output: Estimate of the frequencies $\{f_k\}_{k=1}^X$.

- 1: Set $M_{m,n} = s_{m+n}$ for all $m, n = 1, 2, \dots, N$.
- 2: Perform singular value decomposition on M to obtain $M = USV^\top$.
- 3: **for** $n = 1, \dots, N$ **do**
- 4: If $S_{n,n} > 1$, then $U_{m,n} \rightarrow 0$ for all m .
- 5: **end for**
- 6: Return the local minima of $R(\omega) := \|Ua(\omega)\|_2$.

Algorithm 2 Quench spectroscopy

Input: Initial state ρ , times t , Hamiltonian H , quench operator K , measurement operator M , error bound ε .

Output: Estimate of $Q(\rho, K, M(t))$ with additive error bounded by ε .

- 1: Prepare ρ ;
- 2: Apply quench operator K on the state;
- 3: Let the state evolve under $\exp(-iHt)$;
- 4: Measure the evolved state in the eigenbasis of M ;
- 5: Repeat the procedure for $\mathcal{O}(\varepsilon^{-2})$ times and record the mean value as \bar{Q} .
- 6: Return \bar{Q} .

Algorithm 3 Ancilla-Free Quantum Protocol for Thermal Green's Functions

Input: Hamiltonian H , parity operator P , inverse temperature β , observables A, B , energy gap lower bound ΔE .

Output: Parameters for Green's function $G_{AB}(z)$.

- 1: Let $H_+ = (H + HP)/2$, $H_- = (H - HP)/2$, $\rho_S = e^{-\beta H_+} / \text{Tr}(e^{-\beta H_+})$, and $\rho_A = e^{-\beta H_-} / \text{Tr}(e^{-\beta H_-})$.
- 2: Input $(\rho_\beta, 0, H, I, P, \varepsilon_1)$ to Algorithm 2 and label the output as \hat{p}_T .
- 3: Input $(\rho_S, 0, H, I, P, \varepsilon_1)$ to Algorithm 2 and label the output as \hat{p}_S .
- 4: Input $(\rho_A, 0, H, I, P, \varepsilon_1)$ to Algorithm 2 and label the output as \hat{p}_A .
- 5: Let

$$\hat{r} = \frac{(1 + \hat{p}_A)(1 + \hat{p}_S)(1 - \hat{p}_T)}{(1 - \hat{p}_A)(1 - \hat{p}_S)(1 + \hat{p}_T)}, \quad (\text{S32})$$

$$\hat{N}_S = \dim(H) \frac{\hat{r}}{1 + \hat{r}}, \quad \hat{N}_A = \dim(H) \frac{1}{1 + \hat{r}}, \quad (\text{S33})$$

$$\hat{Z}_S = \hat{N}_A \frac{1 + \hat{p}_S}{1 - \hat{p}_S}, \quad \hat{Z}_A = \hat{N}_S \frac{1 - \hat{p}_A}{1 + \hat{p}_A}. \quad (\text{S34})$$

- 6: **for** $t \in \mathcal{T} = \{1, 2, \dots, \mathcal{O}(\Delta E^{-1})\}$ **do**
- 7: Input $(\rho_\beta, t, H, (I - iA)/\sqrt{2}, B, \varepsilon_2)$ to Algorithm 2 and label the output as $\hat{C}_{t,\text{Im}}$.
- 8: Input $(\rho_S, t, H, (P + A)/\sqrt{2}, B, \varepsilon_2)$ to Algorithm 2 and label the output as $\hat{C}_{t,+,\text{Re}}$.
- 9: Input $(\rho_A, t, H, (P + A)/\sqrt{2}, B, \varepsilon_2)$ to Algorithm 2 and label the output as $\hat{C}_{t,-,\text{Re}}$.
- 10: Input $((I + A)/\dim(H), t, H, I, B, \varepsilon_2)$ to Algorithm 2 and label the output as $\hat{A}_{t,\text{Re}}$.
- 11: Let

$$\hat{C}_t = \frac{\hat{Z}_S + \hat{N}_A}{\hat{Z}_S + \hat{Z}_A} \hat{C}_{t,+,\text{Re}} - \frac{\hat{N}_S + \hat{Z}_A}{\hat{Z}_S + \hat{Z}_A} \hat{C}_{t,-,\text{Re}} + \frac{\dim(H)}{\hat{Z}_S + \hat{Z}_A} \hat{A}_{t,\text{Re}} + i \hat{C}_{t,\text{Im}}. \quad (\text{S35})$$

- 12: **end for**
- 13: Input $\{(t, \hat{C}_t) : t \in \mathcal{T}\}$ to Algorithm 1 and return the output.

S6. ADDITIONAL NUMERICAL RESULTS ON GREEN'S FUNCTIONS

In the main text, we have shown numerical results of the finite-temperature Green's function under strong coupling ($h_U = 6$). Here we further demonstrate the finite-temperature Green's function under weak coupling ($h_U = 0.1$) in Fig. S1, the zero-temperature Green's function under strong (weak) coupling in Figs. S2 (S3), and the finite-temperature Green's function for the 1D XXZ model [see Eq. (7)] in Fig. S4. For the Fermi-Hubbard model at zero-temperature, we show that the excitation spectrum $\{E_n - E_0 : |\langle n | A | 0 \rangle|^2 > 0.01\}$ matches exactly with the local minima of the noise-space correlation function.

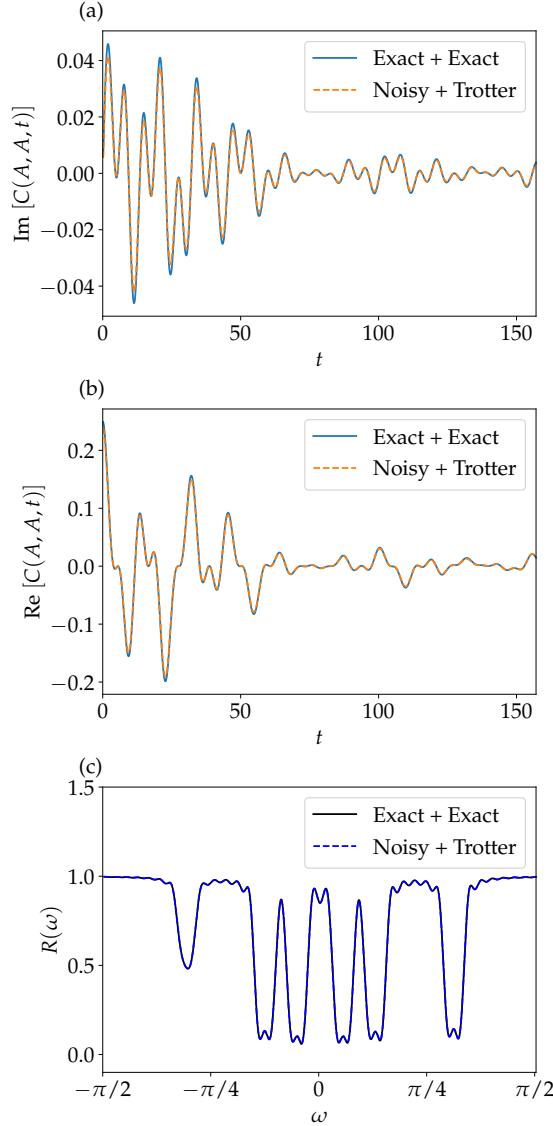


FIG. S1. Finite-temperature Green's function for the 2D Fermi-Hubbard model on a 2×3 lattice without periodic boundary conditions. The initial state is ρ_β with $\beta = 1$, and the interaction strength is $h_U = 0.1$. The observable is $A = B = (c_0 + c_0^\dagger)/2$. The system is evolved up to time 50π with a Trotter step of $\pi/20$. Noise of strength $\varepsilon = 0.1$ is introduced by adding an identical random perturbation ϱ at each time step. In the legend, the first “Exact” denotes an exact initial state, the second “Exact” denotes exact time evolution, “Noisy” corresponds to the perturbed initial state $\rho_\beta + \varepsilon\varrho$ after rescaling, and “Trotter” refers to simulation via the Trotter-Suzuki (TS) decomposition. (a) Imaginary part of $C(A, A, t)$ as a function of time. (b) Real part of $C(A, A, t)$. (c) Comparison of the noise-space correlation function $R(\omega)$ [see SM Eq. (S28)] for $\omega \in [-\pi/2, \pi/2]$. Due to the denoising effect of the MUSIC algorithm, the positions of the local minima of $R(\omega)$ remain unchanged in the noisy model.

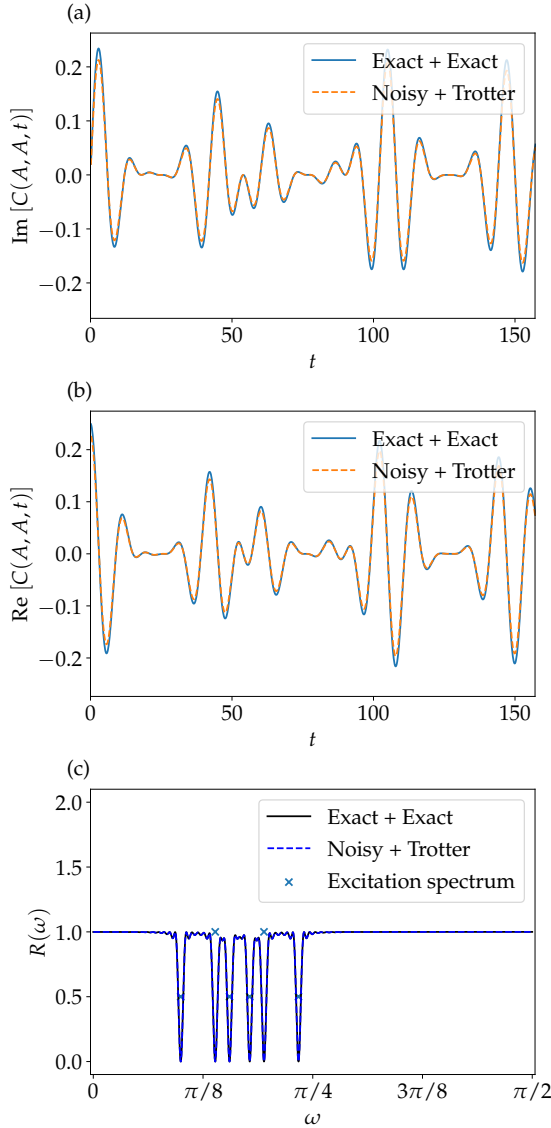


FIG. S2. Ground-state Green's function for the 2D Fermi–Hubbard model on a 2×3 lattice without periodic boundary conditions. The interaction strength is $h_U = 6$. The observable is $A = B = (c_0 + c_0^\dagger)/2$. The system is evolved up to time 200π with a Trotter step of $\pi/20$ (only region $t \in [0, 50\pi]$ is shown in the figure). Noise of strength $\varepsilon = 0.1$ is introduced by adding an identical random perturbation ϱ at each time step. In the legend, the first “Exact” denotes an exact initial state, the second “Exact” denotes exact time evolution, “Noisy” corresponds to the perturbed initial state $\rho_\beta + \varepsilon\varrho$ after rescaling, and “Trotter” refers to simulation via the TS decomposition. (a) Imaginary part of $C(A, A, t)$ as a function of time. (b) Real part of $C(A, A, t)$. (c) Comparison of the noise-space correlation function $R(\omega)$ [see Eq. (S29)] for $\omega \in [0, \pi/2]$. Crosses denote the excitation spectrum $\{E_n - E_0, \alpha_n^2\}$, $\alpha_n \propto |\langle n | A | 0 \rangle|$ for all n , rescaled such that $\max_n \alpha_n = 1$. As shown here, all the energy gaps in the excitation spectrum are captured by the noise-space correlation function, and the impact of the noise is negligible.

S7. TAILORED QUENCH SPECTROSCOPY METHOD FOR OTOC

Out-of-time-order correlator (OTOC) is an important physical quantity in the study of quantum chaos [51, 52]. It quantifies how fast a system scrambles. Suppose ρ is a thermal state, and A, B are two Pauli operators. Then OTOC is defined as

$$\text{OTOC}(A, B, t) := \text{Tr}[\rho A B(t) A B(t)]. \quad (\text{S36})$$

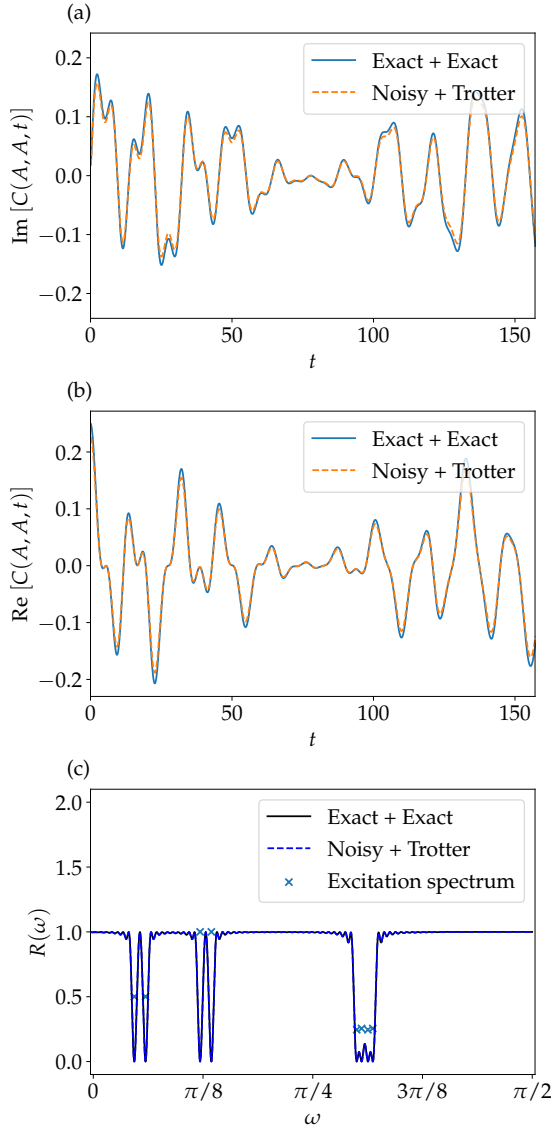


FIG. S3. Ground-state Green's function for the 2D Fermi–Hubbard model on a 2×3 lattice without periodic boundary conditions. The interaction strength is $h_U = 0.1$. The observable is $A = B = (c_0 + c_0^\dagger)/2$. The system is evolved up to time 200π with a Trotter step of $\pi/20$ (only region $t \in [0, 50\pi]$ is shown in the figure). Noise of strength $\varepsilon = 0.1$ is introduced by adding an identical random perturbation ϱ at each time step. In the legend, the first “Exact” denotes an exact initial state, the second “Exact” denotes exact time evolution, “Noisy” corresponds to the perturbed initial state $\rho_\beta + \varepsilon\varrho$ after rescaling, and “Trotter” refers to simulation via the TS decomposition. (a) Imaginary part of $C(A, A, t)$ as a function of time. (b) Real part of $C(A, A, t)$. (c) Comparison of the noise-space correlation function $R(\omega)$ [see Eq. (S29)] for $\omega \in [0, \pi/2]$. Crosses denote the excitation spectrum $\{E_n - E_0, \alpha_n^2\}$, $\alpha_n \propto |\langle n | A | 0 \rangle|$ for all n , rescaled such that $\max_n \alpha_n = 1$. As shown here, all the energy gaps in the excitation spectrum are captured by the noise-space correlation function, and the impact of the noise is negligible.

Note that B can also be regarded as a unitary operator. Let $\tilde{A} := B e^{-iHt} A e^{iHt} B$. Then $\text{OTOC}(A, B, t)$ is equivalent to $C(A, \tilde{A}, t)$. In experiment, all we need is measuring the new quench functions:

$$Q(\rho, K, \tilde{A}(t)) = \text{Tr} \left(K \rho K^\dagger e^{iHt} \tilde{A} e^{-iHt} \right), \quad K = \frac{I + iA}{\sqrt{2}}, \frac{P + A}{\sqrt{2}}. \quad (\text{S37})$$

In fact, any correlation of the form $\text{Tr}(\rho A U B U^\dagger)$ can be realized in a similar way. Here U can be any quantum circuit that commutes with P . For $U = e^{-iHt}$, the full quantum circuit is demonstrated in Fig. S5.

Fig. S6 shows the numerical simulation for a Heisenberg model of the form Eq. (7).

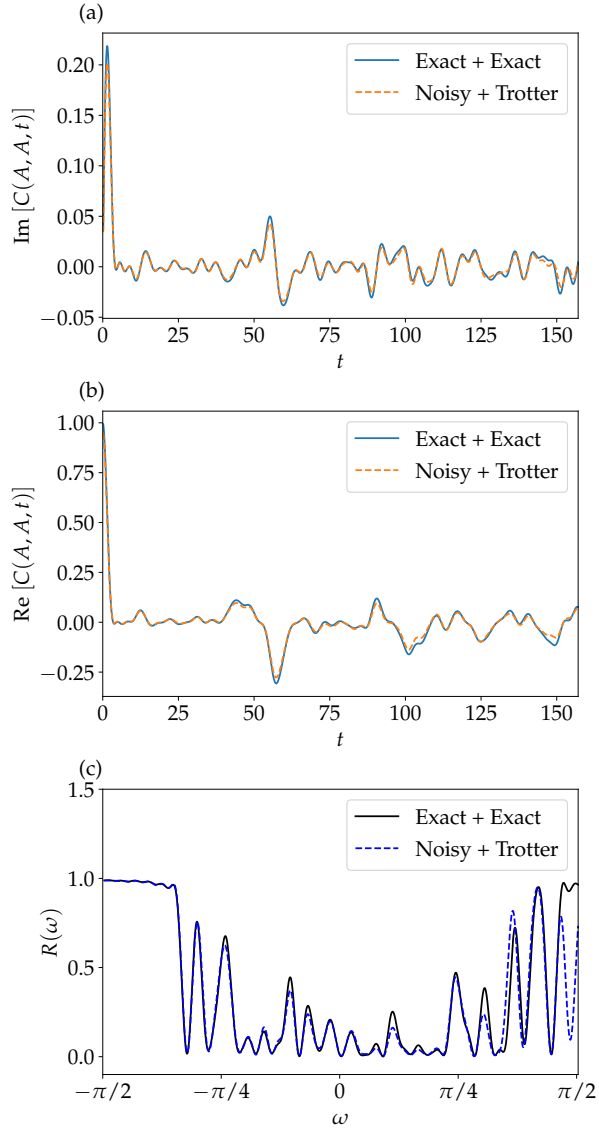


FIG. S4. Finite-temperature Green's function for the 1D XXZ model in Eq. (7) on $N = 8$ sites without periodic boundary condition. The parameters are $J_X = 1$, $J_Z = 2$, and $h = 1$. The initial state is ρ_β with $\beta = 1$. The local observable is $A = B = X_0$. The system is evolved up to time 50π with a Trotter step of $\pi/20$. Noise of strength $\varepsilon = 0.1$ is introduced by adding an identical random perturbation ϱ at each time step. In the legend, the first “Exact” denotes an exact initial state, the second “Exact” denotes exact time evolution, “Noisy” corresponds to the perturbed initial state $\rho_\beta + \varepsilon\varrho$ after rescaling, and “Trotter” refers to simulation via the TS decomposition. (a) Imaginary part of $C(A, A, t)$ as a function of time. (b) Real part of $C(A, A, t)$. (c) Comparison of the noise-space correlation function $R(\omega)$ [see SM Eq. (S28)] for $\omega \in [-\pi/2, \pi/2]$. Due to the denoising effect of the MUSIC algorithm, the positions of the local minima of $R(\omega)$ remain unchanged in the noisy model.

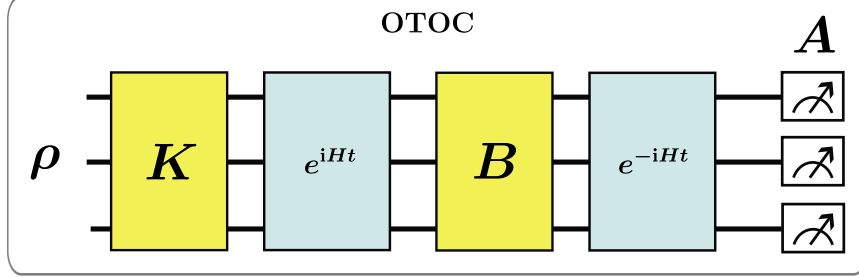


FIG. S5. Quantum circuit for $\text{OTOC}(A, B, t)$ using tailored quench spectroscopy (TQS). If the initial state satisfies $\rho P = \rho$, then choosing $K = (I + iA)/\sqrt{2}$ yields measurement outcomes whose expectation gives $\text{Im}[\text{OTOC}(A, B, t)]$, while setting $K = (P + A)/\sqrt{2}$ provides the real component.

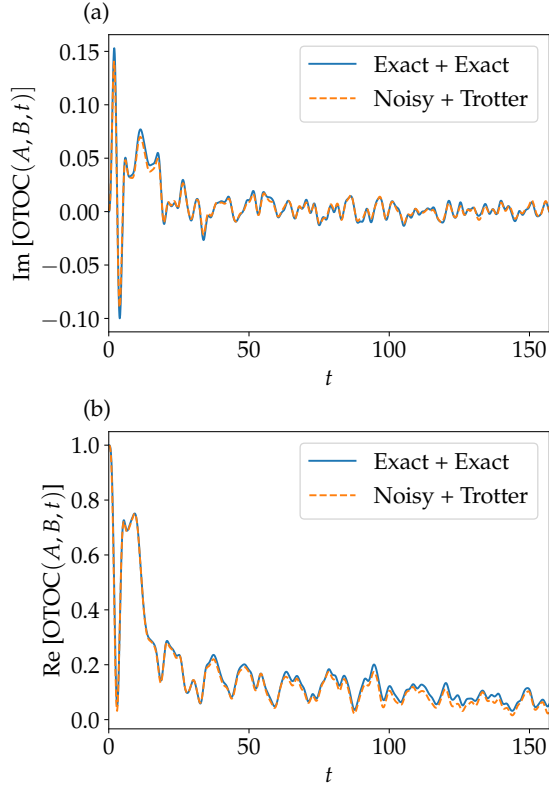


FIG. S6. The real and imaginary components of OTOC for the 1D XXZ model [see Eq. (7)] on $N = 8$ sites without periodic boundary conditions. The parameters are $J_X = 1$, $J_Z = 2$, and $h = 1$. The local observables are $A = X_0$ and $B = Z_2$. The system is evolved up to time 50π with a Trotter step of $\pi/20$. Noise of strength $\varepsilon = 0.1$ is introduced by adding an identical random perturbation ϱ at each time step. In the legend, the first “Exact” denotes an exact initial state, the second “Exact” denotes exact time evolution, “Noisy” corresponds to the perturbed initial state $\rho_\beta + \varepsilon\varrho$ after rescaling, and “Trotter” refers to simulation via the TS decomposition.